

Line Positions and Intensities for the
 $\nu_1 + \nu_2$ and $\nu_2 + \nu_3$ Bands of $^{16}\text{O}_3$

V. Malathy Devi
Department of Physics
College of William and Mary
Williamsburg, Virginia 23185
U.S.A.

J.-M. Flaud and C. Camy-Peyret
Laboratoire de Physique Moléculaire et Atmosphérique
Tour 13, 3^e étage
Université Pierre et Marie Curie et C.N.R.S.
4 place Jussieu
75252 Paris cedex 05
France

C. P. Rinsland and M. A. H. Smith
Atmospheric Sciences Division
NASA Langley Research Center
Hampton, Virginia 23665-5225
U.S.A.

Manuscript pages: 16

Figures: 4

Tables: 2

(NASA-TM-101161) LINE POSITIONS AND
INTENSITIES FOR THE GAMMA 1 + GAMMA 2 AND
GAMMA 2 + GAMMA 3 BANDS OF $(^{16}\text{O})_3$ (NASA)
22 p

CSCL 20L

87 11 11 11
RECEIVED
ALAA
TELETYPE
N88-24542

Unclas
G3/76 0146674

Running title: $\nu_1 + \nu_2$ and $\nu_2 + \nu_3$ Bands of $^{16}\text{O}_3$

Mail Correspondence to:

Dr. V. Malathy Devi
Department of Physics
College of William and Mary
Williamsburg, Virginia 23185

ABSTRACT

Using 0.005-cm^{-1} resolution Fourier transform spectra of $^{16}\text{O}_3$, generated by electric discharge from a $>99.98\%$ pure sample of $^{16}\text{O}_2$, an extensive analysis of the $\nu_1 + \nu_2$ and the $\nu_2 + \nu_3$ bands in the $5.7\ \mu\text{m}$ region was performed. The rotational energy levels of the upper (110) and (011) vibrational states of $^{16}\text{O}_3$ were reproduced within their experimental uncertainties using a Hamiltonian which takes explicitly into account the Coriolis-type interaction occurring between the rotational energy levels of both states. Improved vibrational energies and rotational and coupling constants were also derived for the (110) and (011) states. Precise transition moment constants for these two bands were deduced from analysis of 220 measured line intensities. Finally, a complete list of line positions, intensities, and lower state energies for both bands has been generated.

INTRODUCTION

Because of its atmospheric importance, the $^{16}\text{O}_3$ molecule and the isotopic species $^{16}\text{O}^{18}\text{O}^{16}\text{O}$ and $^{16}\text{O}^{16}\text{O}^{18}\text{O}$ have been the subject of numerous recent spectroscopic studies (1-6 and references therein). Almost all of the recent works were concerned with the pure rotation spectrum and the 10 μm absorption region which are widely used for remote sensing measurements of this molecule in the terrestrial atmosphere. However, absorption by atmospheric ozone is clearly visible in many other spectral regions as well, and we present in this paper our work concerning the 5.7 μm region of $^{16}\text{O}_3$. The prominent bands appearing in this spectral region are the two combination bands $\nu_1 + \nu_2$ and $\nu_2 + \nu_3$. These bands were analyzed in previous laboratory studies (7-9), but at a resolution lower than that achieved in the present work. This work also reports the first experimental measurements of individual line intensities in these bands.

EXPERIMENTAL DETAILS AND ANALYSIS

The ozone samples were prepared using >99.98% pure $^{16}\text{O}_2$. The technique of silent electric discharge was used in generating the ozone. The absorption cell used in these measurements was a 50-cm long 5.08-cm diameter Pyrex tube with Teflon valves. Potassium chloride windows were wedged 5-10 mrad on the cell to prevent channeling arising from multiple reflections. The two spectra used in this analysis were recorded at room temperature with ~ 10.6 and ~ 23.7 Torr of $^{16}\text{O}_3$ in the absorption cell. The sample pressures and temperatures were monitored continuously during the ~ 1 hour scan time for each spectrum using a 0- to 100-Torr Barocel pressure gauge and a thermocouple kept in contact with the cell body. Standards in the ν_3 band of $^{12}\text{C}^{16}\text{O}_2$, reported

by Guelachvili (10) were multiplied by the factor 0.99999979 (average of the two factors reported by Brown et al. (11)) and used to calibrate the wavelength scale of the spectra. For additional experimental details see Flaud et al. (4) and Rinsland et al. (5).

Using the results reported in Ref. (9) it was rather easy to assign transitions with low and medium J and K_a values (up to $J \approx 45$ and $K_a \approx 11$). Following the initial assignments, a first calculation was performed using a Hamiltonian taking into account the Coriolis-type interaction between the rotational levels of the (110) and (011) vibrational states. In this way, an improved set of vibrational energies and rotational and coupling constants was obtained which allowed us to extend the assignments to new lines with higher J and K_a values. The process was repeated until almost all of the $\nu_1 + \nu_2$ and $\nu_2 + \nu_3$ lines observable in the laboratory spectra were assigned. The rotational quantum numbers were extended up to $J < 57$, $K_a < 16$ for $\nu_1 + \nu_2$ and $J < 55$, $K_a < 15$ for $\nu_2 + \nu_3$, thus greatly increasing the previous sets of observed quantum numbers (9). The experimental rotational energy levels of the (110) and (011) upper vibrational states were then obtained by adding the ground state energy levels calculated from the ground state rotational constants given in Ref. (3) to the measured line positions.

THEORETICAL CONSIDERATIONS AND RESULTS

A. Line Positions

According to the energy level scheme of ozone, the (110) and (011) vibrational states of this molecule can be treated as a diad of interacting states and the corresponding Hamiltonian matrix is given in Table I. The v -diagonal part consists of Watson-type Hamiltonians (one for each vibrational state) whereas the off-diagonal part contains operators which take into account the

Coriolis-type interaction affecting the rotational levels of the two interacting states. The experimental energy levels were reproduced quite satisfactorily with this Hamiltonian matrix since a standard deviation of $0.43 \times 10^{-3} \text{ cm}^{-1}$ close to the measurement accuracy was obtained. The vibrational energies, rotational and coupling constants derived from the fit are gathered in Table II and, as noticed in previous works (2, 3, 9), it was not possible to determine simultaneously all the Coriolis coupling constants. Consequently, the $h_{(011,110)}^{c}$ coefficient of the operator iJ_y was fixed to the value previously used (3) for the (001) and (100) vibrational states of $^{16}\text{O}_3$.

From the diagonalization of the Hamiltonian matrix, it was easy to obtain the vibration-rotation wavefunctions which can be written as:

$$|v_1 v_2 v_3 \ J \ K_a K_c \rangle = \sum_{v=(110),(011)} \sum_K C_K^v |v \rangle |J \ K \ \gamma \rangle \quad (1)$$

where the $|J \ K \ \gamma \rangle$'s are Wang functions:

$$|J \ K \ \gamma \rangle = \frac{1}{\sqrt{2}} (|J \ K \rangle + \gamma |J - K \rangle) \quad K > 0, \ \gamma = \pm 1$$

$$|J \ 0 \ + \rangle = |J \ 0 \ \rangle. \quad (2)$$

From the wavefunction of a given vibrational level it is possible to calculate the mixing coefficient, $\% (v)$ on the state $|v \rangle$ of this level, which is given by

$$\% (v) = \sum_K |C_K^v|^2. \quad (3)$$

This coefficient indicates whether the level is affected by a resonance or not. We have plotted in Fig. 1 the mixing coefficients of some (011) rotational levels and the following observations can be made:

- a. There is a smooth behavior of the mixing coefficients with J for the series of levels with $K_a = 12, 13, 14, 15,$ and 16 .
- b. Contrary to the above series, the $K_a = 5$ series is not regular. The large value of the mixing coefficient at $J = 39$ results from the accidental proximity of the resonating (110) [39 2 38] and the (011) [39 5 34] rovibrational levels.

B. Line Intensities

Using the equivalent width method, about 220 line intensities were measured with an average relative uncertainty of 10%. Although the two spectra described previously were used for the band analysis, only the higher pressure (~23.7 Torr) spectrum was used for intensity measurements. This is because many lines were too weak to be measured accurately in the lower abundance spectrum. Because the exact amount of ozone in the cell was not known, we decided to calibrate the intensities of the $\nu_1 + \nu_2$ and $\nu_2 + \nu_3$ bands of ozone with respect to intensities measured in the 10 μm region which contains the ν_3 and ν_1 bands (3). Consequently, we have measured from the same spectrum 95 ν_1 line intensities which were calibrated using the results of Ref. (3). In this way, the intensities in the 5.7 μm region ($\nu_1 + \nu_2$ and $\nu_2 + \nu_3$ bands) are consistent with the intensities in the 10 μm region (ν_1 and ν_3 bands). The $\nu_1 + \nu_2$ and $\nu_2 + \nu_3$ experimental relative intensities were then reproduced using the following transformed transition moment operators (see Ref. 12 for detailed explanations):

$\nu_1 + \nu_2$ (B-type Band)

$$\begin{aligned} (000)(110) \mu'_z &= (-0.5054_6 \pm 0.0025) \times 10^{-2} \phi_x \\ &+ (-0.113_2 \pm 0.021) \times 10^{-4} \{i\phi_y, J_z\} \\ &+ (0.514_9 \pm 0.010) \times 10^{-4} \{\phi_z, iJ_y\} + \dots \end{aligned} \quad (4)$$

$\nu_2 + \nu_3$ (A-type Band)

$$\begin{aligned} (000)(011) \mu'_z &= (-0.9081_3 \pm 0.0050) \times 10^{-2} \phi_z \\ &+ (0.93_4 \pm 0.21) \times 10^{-5} \frac{1}{2} [\{\phi_x, iJ_y\} - \{i\phi_y, J_x\}] \\ &+ (0.93_3 \pm 0.43) \times 10^{-5} \frac{1}{2} [\{\phi_x, iJ_y\} + \{i\phi_y, J_x\}] + \dots \end{aligned} \quad (5)$$

with $\{A, B\} = AB + BA$

$\phi_\alpha = \phi_{z\alpha}$ (direction cosine)

$J_\alpha =$ component of J along the molecular axis α .

All of the results are given in Debye.

The statistical analysis of the results is as follows:

$0 < \frac{\delta I}{I_{\text{obs.}}} < 10\%$	69.1% of the lines
$10 < \frac{\delta I}{I_{\text{obs.}}} < 20\%$	24.8% of the lines
$20 < \frac{\delta I}{I_{\text{obs.}}} < 30\%$	6.1% of the lines.

where $\delta I = |I_{\text{obs.}} - I_{\text{calc.}}|$, $I_{\text{obs.}}$ is the observed, and $I_{\text{calc.}}$ is the calculated intensity.

These results are very satisfactory since 69% of the intensities are reproduced within the experimental uncertainty of 10%. The following points of the analysis are of interest:

1) Since the line intensities are proportional to the square of the dipole moment matrix elements, only the relative signs of the transition moment constants are determined. A method to obtain their absolute signs (signs with respect to the permanent dipole moment of the molecule) would be to study the hot bands $\nu_1 - \nu_2$ and $\nu_3 - \nu_2$ as was done for the water molecule (13).

2) The constants, coefficients of ϕ_x and ϕ_z , are of the same order of magnitude which implies that the $\nu_1 + \nu_2$ band is almost as intense as the $\nu_2 + \nu_3$ band, which is not very common. Usually, for ozone, in a given spectral region the A-type band is much stronger than the B-type band (see the 10 μm region for example).

3) The rotational correcting terms are not negligible particularly for the B-type band. In fact, these terms allow the calculation to reproduce quite satisfactorily the intensity peculiarities which were noted in Ref. (9).

Finally, using the vibrational energies and the rotational and coupling constants given in Table II as well as the transition moment constants given in Eq. (4) and (5), we have generated a list of 7110 line positions and intensities for the $\nu_1 + \nu_2$ and $\nu_2 + \nu_3$ bands of ozone. The calculations were performed¹ using an intensity cut-off of $0.1 \times 10^{-24} \text{ cm}^{-1}/\text{molecule cm}^{-2}$ at 296 K, maximum values of 70 for J and 21 for K_a , and a maximum lower state energy of 3000 cm^{-1} . Total band intensities of 0.237×10^{-19} and $0.536 \times 10^{-19} \text{ cm}^{-1}/\text{molecule cm}^{-2}$ at 296 K were obtained respectively for

¹ A partition function $Z(296) = 3473$ was used in the intensity calculations.

the $\nu_1 + \nu_2$ and $\nu_2 + \nu_3$ bands of $^{16}\text{O}_3$. These results agree within 10% with the low resolution integrated band intensities reported in Ref. (7), which is quite satisfactory.

Figures 2 to 4 show comparisons of the measured and calculated spectra in three different spectral regions. In all cases the observed features of the $\nu_1 + \nu_2$ and the $\nu_2 + \nu_3$ bands are reproduced very well by the calculations. The weak unassigned lines in Figure 2, marked by solid triangles, are believed to be transitions of the $2\nu_2 + \nu_3 - \nu_2$ hot band. Similarly, the few unassigned absorptions marked by solid triangles in Figure 3 are probably lines of the $2\nu_1 + \nu_2 - \nu_2$ hot band. These hot band lines are about 5% as strong as the strongest lines of the $\nu_1 + \nu_2$ and the $\nu_2 + \nu_3$ bands. Because of the weakness of the hot band lines in the present spectra and the absence of assignments for the $2\nu_2 + \nu_3$ and the $2\nu_1 + \nu_2$ bands, analysis of these features has not been attempted at this time. It should be emphasized that the absolute values of the intensities calculated here for the $\nu_1 + \nu_2$ and $\nu_2 + \nu_3$ bands have been calibrated against intensities from the 10 μm spectral region which have been obtained assuming the value $\left(\frac{\partial\mu_z}{\partial q_3}\right)_e = -0.2662 \text{ D}$ (see Ref. 3 for more details).

ACKNOWLEDGMENTS

The authors thank Charles T. Solomon of NASA Langley and Rob Hubbard and Jeremy Wagner of the National Solar Observatory (NSO) for their help with the laboratory experiment, Gregg Ladd for the computer processing of the data at NSO, and D. Chris Benner of William and Mary and Carolyn H. Sutton of SASC Technologies for their assistance in the processing of the spectra at NASA Langley. Research at the College of William and Mary was supported under Cooperative Agreement NCC 1-80 with NASA. C. Camy-Peyret and J.-M. Flaud acknowledge partial support of their research work under USAF Agreement

RES D5-674. The National Solar Observatory is operated by the Association of Universities for Research in Astronomy, Inc., under contract with the National Science Foundation. The computational work was performed at the Centre Inter Regional de Calcul Electronique, CNRS, 91405 Orsay, France.

TABLE I

Hamiltonian matrices

v = (110)	v' = (011)	
Watson-type Hamiltonian	Hermitic conj.	v = (000)
$H_{v,v}$		Watson-type Hamiltonian
Coriolis interaction	Watson-type Hamiltonian	$H_{v,v}$
$H_{v,v}^c$	$H_{v',v'}$	

$$H_{v,v} = E_v$$

$$\begin{aligned}
 & + \left[A^v - \frac{1}{2}(B^v + C^v) \right] J_z^2 + \frac{1}{2}(B^v + C^v) J^2 + \frac{1}{2}(B^v - C^v) J_{xy}^2 \\
 & - \Delta_K^v J_z^4 - \Delta_{JK}^v J_z^2 J^2 - \Delta_J^v (J^2)^2 - \delta_K^v \left\{ J_z^2, J_{xy}^2 \right\} - 2\delta_J^v J_{xy}^2 J^2 \\
 & + H_K^v J_z^6 + H_{KJ}^v J_z^4 J^2 + H_{JK}^v J_z^2 (J^2)^2 + H_J^v (J^2)^3 \\
 & + h_K^v \left\{ J_z^4, J_{xy}^2 \right\} + h_{KJ}^v \left\{ J_z^2, J_{xy}^2 \right\} J^2 + 2h_J^v J_{xy}^2 (J^2)^2 \\
 & + L_K^v J_z^8 + L_{KKJ}^v J_z^6 J^2 + L_{KJ}^v J_z^4 (J^2)^2 + L_{KJJ}^v J_z^2 (J^2)^3 + L_J^v (J^2)^4 \\
 & + I_K^v \left\{ J_z^6, J_{xy}^2 \right\} + I_{KJ}^v \left\{ J_z^4, J_{xy}^2 \right\} J^2 + I_{JK}^v \left\{ J_z^2, J_{xy}^2 \right\} (J^2)^2 + 2I_J^v J_{xy}^2 (J^2)^3 \\
 & + P_K^v J_z^{10} + P_{KKKJ}^v J_z^8 J^2 + P_{KKJ}^v J_z^6 (J^2)^2 + \dots \\
 & + P_K^v \left\{ J_z^8, J_{xy}^2 \right\} + P_{KKJ}^v \left\{ J_z^6, J_{xy}^2 \right\} J^2 + \dots
 \end{aligned}$$

$$\begin{aligned}
 H_{v,v}^c & = h_{v,v}^c \{ J_x, J_y \} + h_{v,v}^{\prime c} i J_y + h_{v,v}^{\prime\prime c} \left\{ J_z^2, \{ J_x, J_z \} \right\} \\
 & + h_{v,v}^{\prime\prime\prime c} \{ J_x, J_z \} J^2 + h_{v,v}^{\prime\prime\prime\prime c} \left(J_-^3 - J_+^3 \right)
 \end{aligned}$$

with $\{A, B\} = AB + BA$

$$\begin{aligned}
 J_{xy}^2 & = J_x^2 - J_y^2 \\
 J_{\pm} & = J_x \mp i J_y
 \end{aligned}$$

Table II. Vibrational energies, rotational and coupling constants
for the (110) and (011) vibrational states of $^{16}\text{O}_3$

Vibrational and Rotational Constants		
	(110)	(011)
E_v	$1796.26187_0 \pm 0.000057$	$1726.52249_0 \pm 0.000075$
A^v	$3.6108121_{34} \pm 0.0000035$	$3.5523057_{11} \pm 0.0000053$
B^v	$0.44144616_{08} \pm 0.00000050$	$0.43989711_{75} \pm 0.00000055$
C^v	$0.39029870_{66} \pm 0.00000043$	$0.38850339_{96} \pm 0.00000046$
Δ_K^v	$(0.239727_{92} \pm 0.000068) \times 10^{-3}$	$(0.22865_{41} \pm 0.00012) \times 10^{-3}$
Δ_{KJ}^v	$(-0.20752_{54} \pm 0.00091) \times 10^{-5}$	$(-0.1598_{22} \pm 0.0011) \times 10^{-5}$
Δ_J^v	$(0.46689_{33} \pm 0.00025) \times 10^{-6}$	$(0.45985_{71} \pm 0.00023) \times 10^{-6}$
δ_K^v	$(0.4321_{19} \pm 0.0042) \times 10^{-5}$	$(0.3495_{31} \pm 0.0010) \times 10^{-5}$
δ_J^v	$(0.6472_{74} \pm 0.0020) \times 10^{-7}$	$(0.7609_{92} \pm 0.0023) \times 10^{-7}$
H_K^v	$(0.4996_{50} \pm 0.0048) \times 10^{-7}$	$(0.464_{48} \pm 0.010) \times 10^{-7}$
H_{KJ}^v	$(-0.2103_{52} \pm 0.0059) \times 10^{-8}$	$(-0.1875_{97} \pm 0.0027) \times 10^{-8}$
H_{JK}^v	$(-0.83_{76} \pm 0.13) \times 10^{-10}$	$(-0.311_{10} \pm 0.023) \times 10^{-10}$
H_J^v	$(0.169_{22} \pm 0.079) \times 10^{-12}$	$(0.113_{62} \pm 0.059) \times 10^{-12}$
h_K^v	$(-0.27_{93} \pm 0.11) \times 10^{-8}$	
h_{KJ}^v	$(-0.33_{01} \pm 0.16) \times 10^{-10}$	
h_J^v	$(0.91_{60} \pm 0.53) \times 10^{-13}$	$(0.199_{99} \pm 0.059) \times 10^{-12}$
L_K^v	$(-0.126_{35} \pm 0.010) \times 10^{-10}$	$(-0.107_{62} \pm 0.027) \times 10^{-10}$
L_{KKJ}^v	0.2739×10^{-12}	0.2739×10^{-12}
L_{JJK}^v	-0.3251×10^{-15}	-0.3251×10^{-15}
L_J^v	0.2994×10^{-17}	0.2994×10^{-17}
l_K^v	0.1812×10^{-12}	0.1812×10^{-12}

Table II. Concluded

	(110)	(011)
P_K^V	0.333×10^{-14}	0.333×10^{-14}
P_{KKKJ}^V	0.1895×10^{-15}	0.1895×10^{-15}
Coupling Constants		
	$h_{(011)(110)}^C = (-0.10099_{76} \pm 0.00016) \times 10^{-1}$	
	$h'_{(011)(110)} = -0.470$	
	$h''_{(011)(110)} = (0.855_{10} \pm 0.046) \times 10^{-6}$	
	$h'''_{(011)(110)} = (-0.1062_{48} \pm 0.0063) \times 10^{-6}$	
	$h''''_{(011)(110)} = (-0.59_{31} \pm 0.23) \times 10^{-8}$	

All the results are in cm^{-1} and the quoted errors are one standard deviation. The constants without errors were held fixed during the calculation; they come from Ref. (3).

REFERENCES

1. M. Carlotti, G. Di Lonardo, L. Fusina, A. Trombetti, A. Bonetti, B. Carli, and F. Mencaraglia, *J. Mol. Spectrosc.* 107, 89-93 (1984).
2. H. M. Pickett, E. A. Cohen, and J. S. Margolis, *J. Mol. Spectrosc.* 110, 186-214 (1985).
3. J.-M. Flaud, C. Camy-Peyret, V. Malathy Devi, C. P. Rinsland and M. A. H. Smith, *J. Mol. Spectrosc.* (submitted).
4. J.-M. Flaud, C. Camy-Peyret, V. Malathy Devi, C. P. Rinsland, and M. A. H. Smith, *J. Mol. Spectrosc.* 118, 334-344 (1986).
5. C. P. Rinsland, V. Malathy Devi, J.-M. Flaud, C. Camy-Peyret, M. A. H. Smith, and G. M. Stokes, *J. Geophys. Res.* 90, 10719-10725 (1985).
6. C. Camy-Peyret, J.-M. Flaud, A. Perrin, V. Malathy Devi, C. P. Rinsland, and M. A. H. Smith, *J. Mol. Spectrosc.* 118, 345-354 (1986).
7. D. J. McCaa and J. H. Shaw, *J. Mol. Spectrosc.* 25, 374-397 (1968).
8. C. Jones and J. H. Shaw, *J. Mol. Spectrosc.* 68, 48-55 (1977).
9. A. Barbe, C. Secroun, P. Jouve, C. Camy-Peyret, and J.-M. Flaud, *J. Mol. Spectrosc.* 75, 103-110 (1979).
10. G. Guelachvili, *J. Mol. Spectrosc.* 79, 72-83 (1980).
11. L. R. Brown and R. A. Toth, *J. Opt. Soc. Am.* B2, 842-856 (1985).
12. J.-M. Flaud, C. Camy-Peyret, and R. A. Toth, "Water vapor line parameters from microwave to medium infrared", Pergamon Press, Oxford (1981).
13. C. Camy-Peyret and J.-M. Flaud, in "Molecular Spectroscopy: Modern Research", vol. III (K. Narahari Rao, Ed.), Academic Press, Orlando (1985).

List of Symbols

- ν - lower case Greek nu
- μ - lower case Greek mu
- δ - lower case Greek delta
- θ - lower case Greek theta
- ϕ - lower case Greek phi
- Δ - upper case Greek delta
- ∂ - symbol for partial derivative
- α - lower case Greek alpha
- γ - lower case Greek gamma

Figure Captions

Figure 1. Mixing coefficients in % (110) for some rotational levels of the (011) state. For high K_a values, the mixing coefficients vary smoothly with J ; a crossing of levels occurs for $K_a = 14, 15,$ and 16 . For $K_a = 5$, the mixing is weak except for $J = 39$; the large mixing coefficient is caused by the accidental proximity of the (110) [39 2 38] and the (011) [39 5 34] rovibrational levels.

Figure 2. Laboratory (solid line) and best-fit calculated (crosses) spectra in the region of the $\nu_2 + \nu_3$ band around 1682 cm^{-1} (lower panel). The laboratory spectrum was recorded with about 23.7 Torr of $^{16}\text{O}_3$ in a 50-cm long absorption path at room temperature. Residuals (observed minus calculated) are shown in the upper panel. The $\nu_1 + \nu_2$ line [39 2 38] + [40 5 35] located at 1681.838 cm^{-1} appears only because it borrows its intensity from the $\nu_2 + \nu_3$ line [39 5 34] + [40 5 35] at 1682.007 cm^{-1} . Although the $\Delta K_a = 3$ $\nu_1 + \nu_2$ line is blended by a weaker hot band line, it can be seen that the intensities of the two resonating lines are almost equal because of a mixing coefficient of about 50% (see Figure 1). Several high K_a lines of the $\nu_2 + \nu_3$ band (marked with an asterisk) are also observable in this region. Unassigned absorptions in this region are believed to be from the $2\nu_2 + \nu_3 - \nu_2$ hot band and are indicated by solid triangles.

Figure 3. Laboratory (solid line) and best-fit calculated (crosses) spectra in the region of the $\nu_1 + \nu_2$ band around 1832 cm^{-1} (lower panel). The laboratory spectrum was recorded with about 23.7 Torr of $^{16}\text{O}_3$ in a 50-cm absorption path at room temperature. Residuals

(observed minus calculated) are shown in the upper panel. High J lines of the $\nu_1 + \nu_2$ band (*) are observed in this spectral region. Their absorption is well reproduced by the calculations. Weak unassigned lines in this region are believed to be from the $2\nu_1 + \nu_2 - \nu_2$ hot band and are indicated by solid triangles.

Figure 4. Laboratory (solid line) and best-fit calculated (crosses) spectra in the region of the $\nu_1 + \nu_2$ band around 1860 cm^{-1} (lower panel). The laboratory spectrum was recorded with about 23.7 Torr of $^{16}\text{O}_3$ in a 50-cm long absorption path at room temperature. Residuals (observed minus calculated) are shown in the upper panel. The $R_{Q_{K''}=10}$ line series (*) is clearly visible and is well reproduced by the calculations.

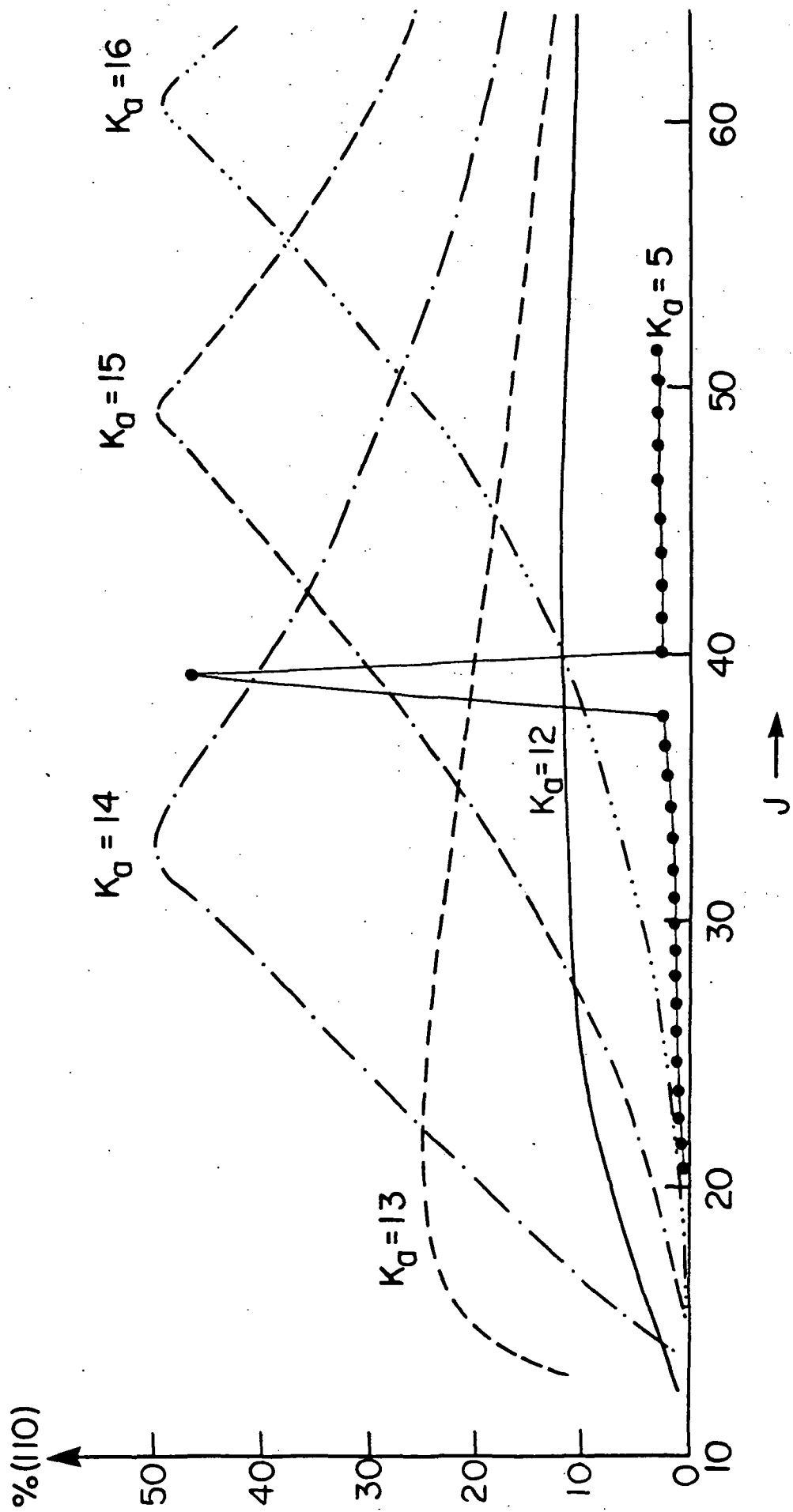


Fig. 1

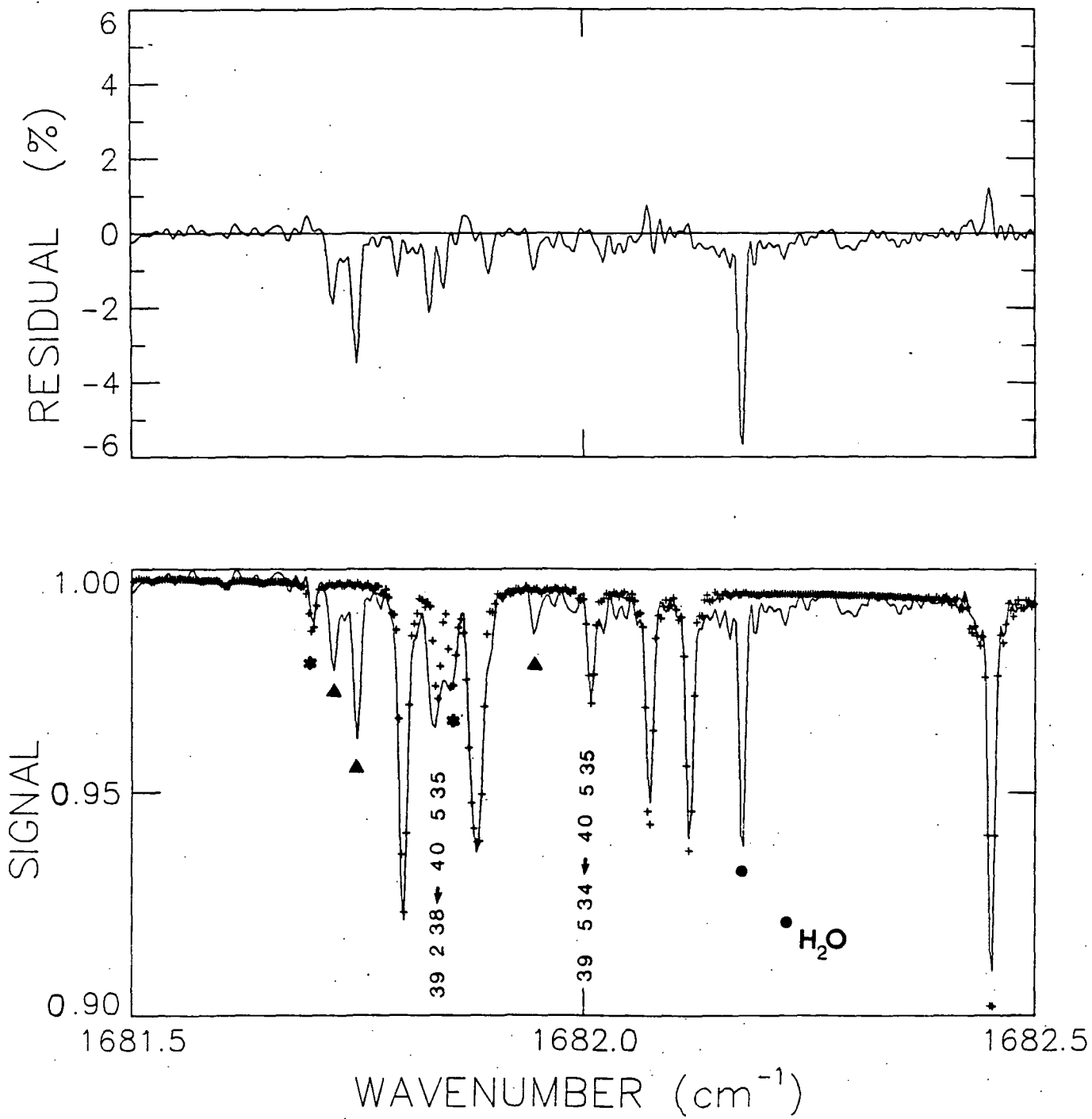


Fig. 2

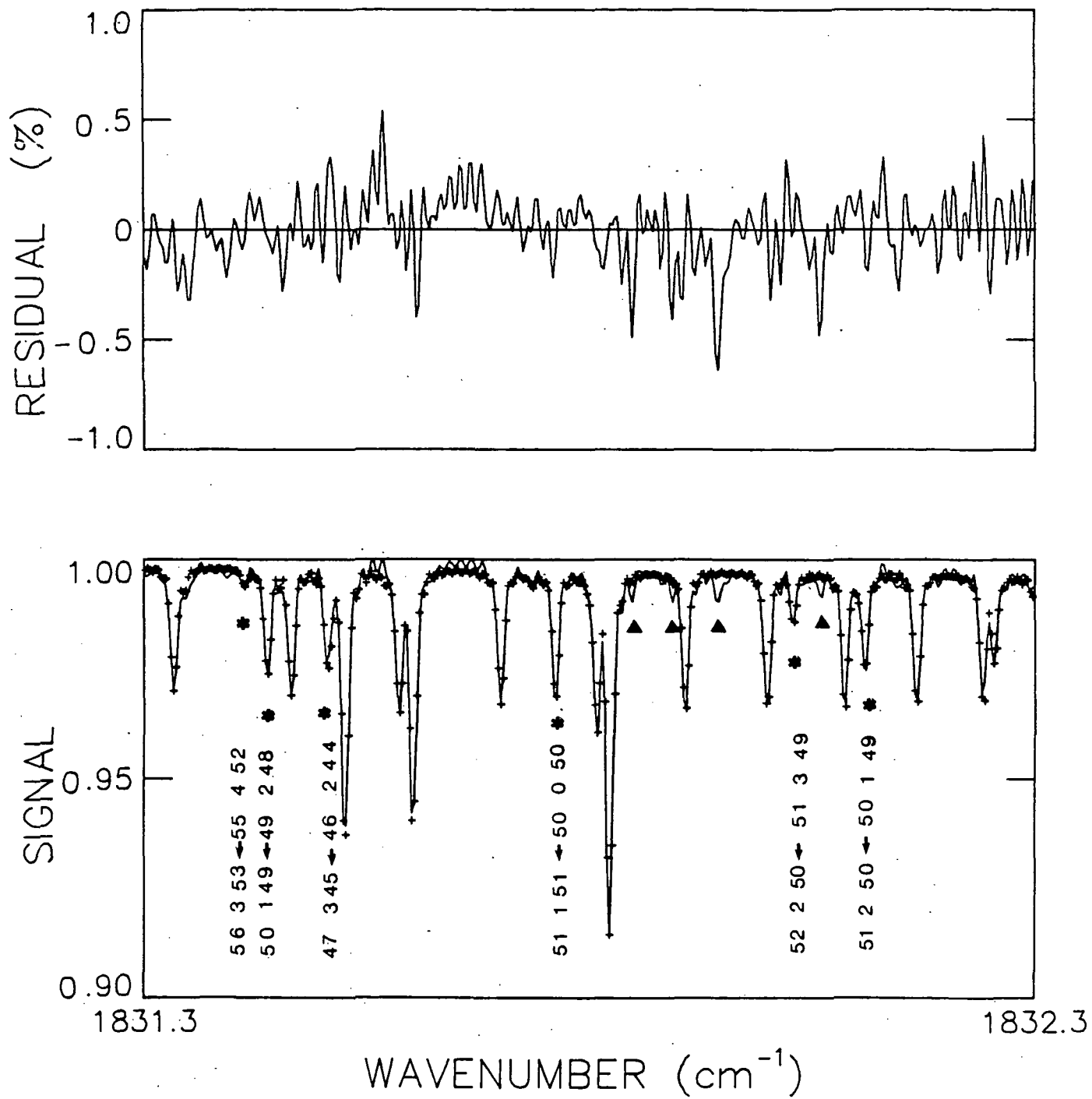


Fig. 3

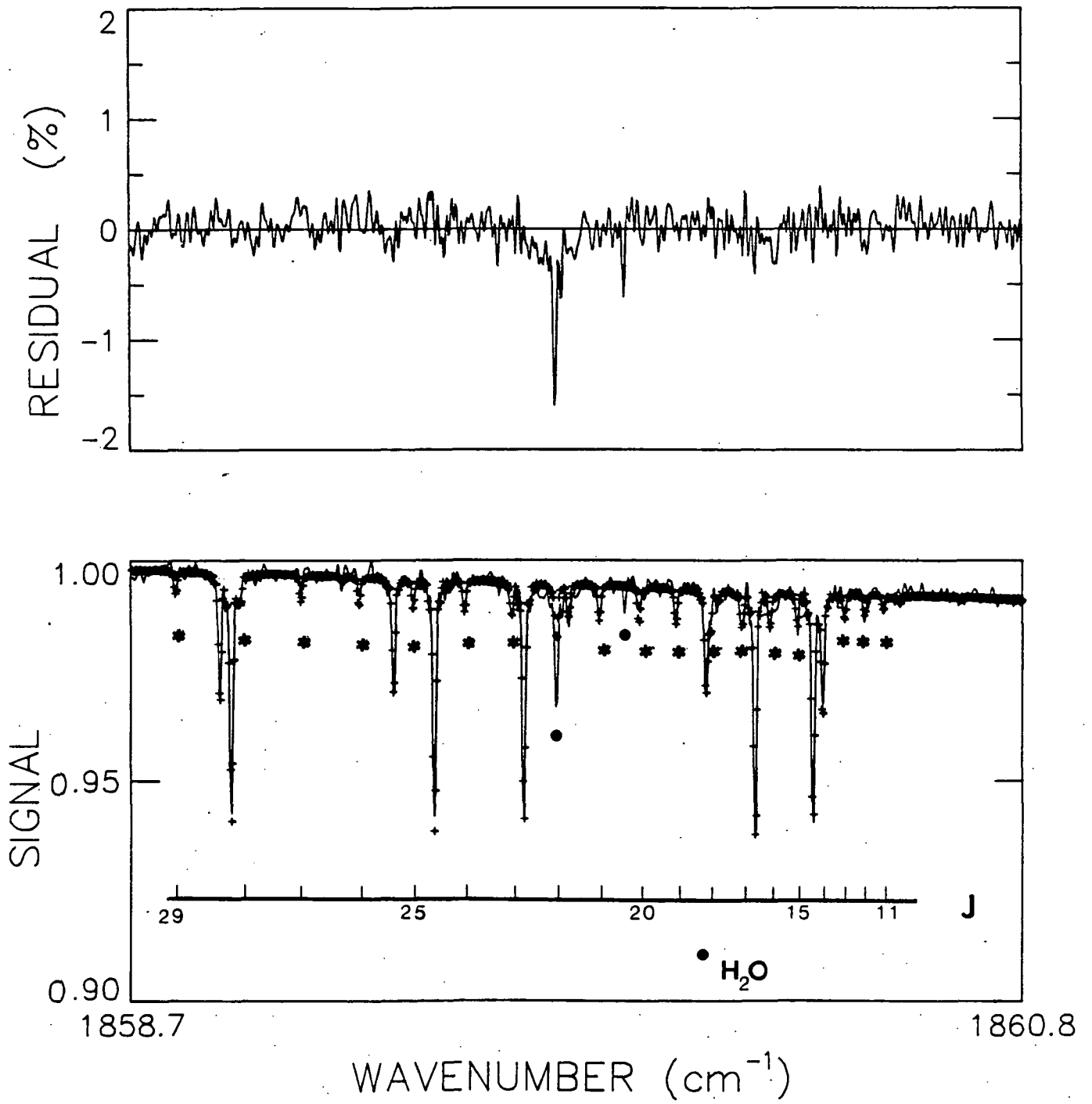


Fig. 4